IEEE Photonics Journal
An IEEE Photonics Society Publication

Open Access

Apodized Focusing Fully Etched Subwavelength Grating Couplers

Volume 7, Number 3, June 2015

Yun Wang
Han Yun
Zeqin Lu
Richard Bojko
Wei Shi
Xu Wang
Jonas Flueckiger
Fan Zhang
Michael Caverley
Nicolas A. F. Jaeger
Lukas Chrostowski

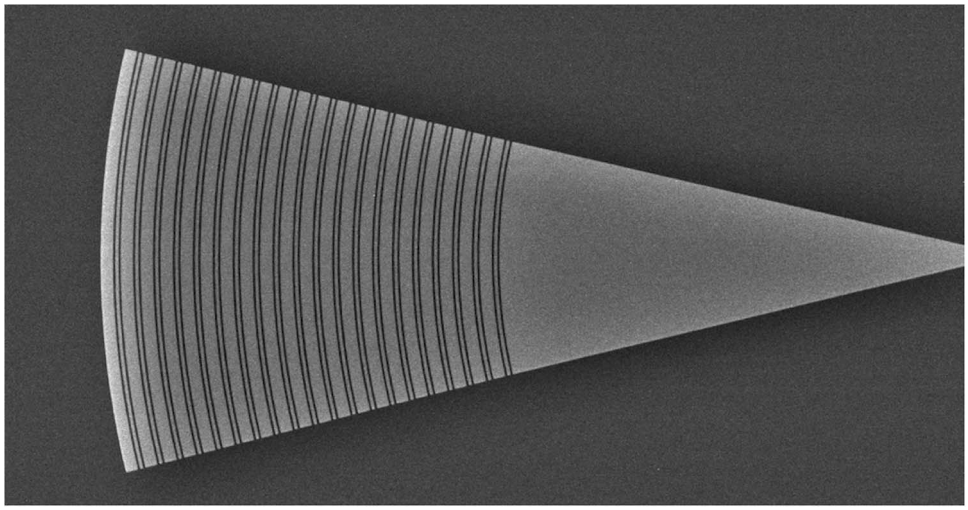

DOI: 10.1109/JPHOT.2015.2426879
1943-0655

IEEE photonics SOCIETY

IEEE

Apodized Focusing Fully Etched Subwavelength Grating Couplers

Yun Wang,[1] Han Yun,[1] Zeqin Lu,[1] Richard Bojko,[2] Wei Shi,[3] Xu Wang,[4] Jonas Flueckiger,[1] Fan Zhang,[1] Michael Caverley,[1] Nicolas A. F. Jaeger,[1] and Lukas Chrostowski[1]

[1]Department of Electrical and Computer Engineering, University of British Columbia, Vancouver, BC V6T 1Z4, Canada
[2]Department of Electrical Engineering, University of Washington, Seattle, WA 98195 USA
[3]Department of Electrical and Computer Engineering, Université Laval, Québec, QC G1V 0A6, Canada
[4]Lumerical Solutions, Vancouver, BC V6E 3L2, Canada

DOI: 10.1109/JPHOT.2015.2426879

Manuscript received March 26, 2015; revised April 20, 2015; accepted April 21, 2015. Date of publication April 29, 2015; date of current version May 12, 2015. This work was supported by the Natural Sciences and Engineering Research Council of Canada through the CREATE SiEPIC program.
Corresponding author: Y. Wang (e-mail: oscar.yunwang@gmail.com).

Abstract: We experimentally demonstrate apodized focusing subwavelength grating couplers for both the fundamental transverse electric (TE_{00}) mode and the fundamental transverse magnetic (TM_{00}) mode. A measured insertion loss of 3.2 dB with a 1-dB bandwidth of 36 nm has been obtained for the TE_{00} mode, and a measured insertion loss of 3.3 dB with a 1-dB bandwidth of 37 nm has been obtained for the TM_{00} mode. Back reflections of −24 dB and −21 dB have been obtained for the TE_{00} and TM_{00} modes, respectively.

Index Terms: Subwavelength structures, gratings.

1. Introduction

Silicon-on-Insulator (SOI), with a high index contrast between the silicon layer and its cladding, provides an unprecedented opportunity to make highly integrated photonics circuits with submicron silicon-wire waveguides. However, the small feature sizes of the waveguides results in severe mode mismatch between the optical fiber and the waveguide. Grating couplers provide a solution to address the mode mismatch issue with the advantages of low cost, space efficiency, and alignment simplicity. Surface coupled grating couplers also enable chip-scale or wafer-scale automated testing, which is a major advantage over the alternatives. Highly efficient shallow etched grating couplers have been achieved on SOI through CMOS foundries [1]–[3]. However, the long turn-around time and the requirement for design rule checking make fabrication through CMOS foundries less attractive for prototyping than electron beam fabrication. Fabrication through high quality electron-beam lithography, with short turn-around time and low cost, offers solution for rapid prototyping of silicon photonics devices and circuits. Compared to the fabrication of fully etched grating couplers, fabricating shallow etched grating couplers with various etch depths increases both the fabrication complexity and cost. Fully etched grating couplers with subwavelength structures have been explored in recent years [4]–[7]. However, all of the

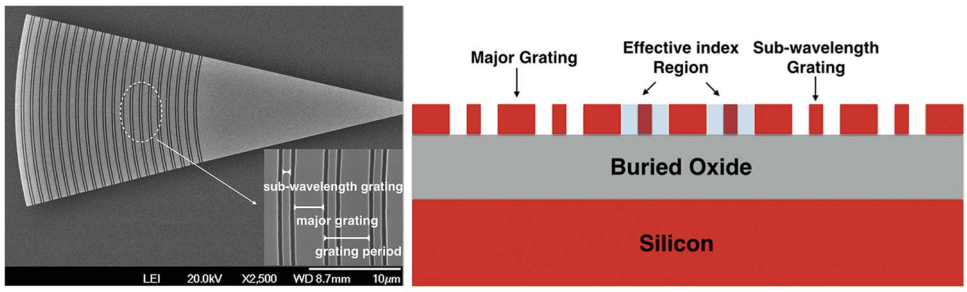

Fig. 1. (a) SEM image of a focusing SWGC. (b) Schematic of the cross-section view of the SWGC.

above designs used straight gratings where adiabatic tapers on the order of a few hundred microns were required to couple the light within the grating into the silicon-wire waveguide modes. Space-efficient designs with focusing subwavelength grating couplers (SWGCs) have also been attempted [8]–[10], however, the oscillation ripples caused by the back reflections from those grating couplers need to be reduced.

Compact SWGCs, with effective index regions achieved using subwavelength grating lines, have been demonstrated in [11]. It is advantageous to use subwavelength grating lines, as compared to traditional quasi-squares, to achieve the effective index regions in SWGCs for several reasons. From the fabrication perspective, the subwavelength grating lines are less challenging to produce because they benefit from higher exposure contrasts [11] and shorter fabrication times, resulting in high fabrication accuracy and lower fabrication cost. From the design perspective, due to our use of subwavelength grating lines that stretch the entire width of the coupler, our SWGCs are simple and straightforward to draw and subsequently, to simulate in both 2-D and 3-D. By contrast, virtual effective index regions have been used in 2-D simulations to approximate the effective index regions in SWGCs using quasi-squares, which over simplifies the situation and results in mismatches between simulations and measurements. Only uniform gratings have been used in [11] where further improvement can be made by apodizing the grating period to achieve better mode match between the grating and the fiber. The maximum theoretical coupling efficiency for a grating coupler with uniform gratings is nearly 80% [12], which means that there may be up to a 1-dB room for improvement by using non-uniform gratings. In this paper, we compared two different approaches to apply apodization to our SWGCs, and we experimentally demonstrate fully etched SWGCs with apodized grating periods and focusing grating lines for both the TE_{00} and the TM_{00} modes.

2. Design and Simulation

Our grating couplers are designed based on SOI wafers with 220 nm silicon and 3 μm buried silicon dioxide (BOX) layers. A scanning electron microscope (SEM) image and a schematic of a cross-section of our fully etched SWGC are shown in Fig. 1. Our fully etched grating coupler consists of two types of gratings, the major gratings and the subwavelength gratings. The subwavelength gratings are small enough for the optical wave to see them as “averaged” effective index regions, so that the back reflection of the grating coupler determined by the Fresnel reflection can be dramatically reduced.

2.1. Incident Angle

The incident angle of a SWGC is determined by the phase-match condition between the grating mode and the fiber mode. As shown in Fig. 2, if we denote θ as the incident angle, which is defined as the angle between the direction of the out-coupled wave and the normal

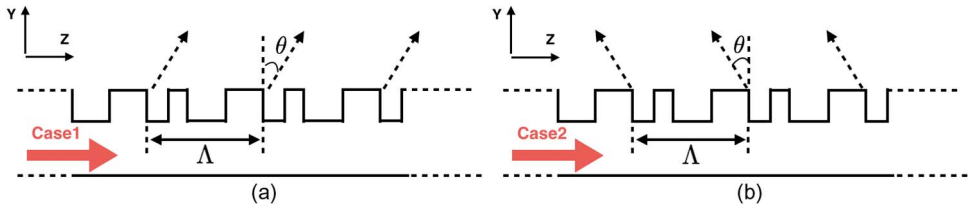

Fig. 2. Schematic of the cross section of a SWGC with (a) a positive incident angle and (b) a negative incident angle.

TABLE 1

Parameters of the uniform SWGCs

PI	WI (nm)	Angle (°)	Period (nm)	Grating$_w$ (nm)	Sub$_w$ (nm)
TE	1550	-31	556	260	78
TM	1550	10	960	575	140

to the grating and Λ as the period of the grating, then the phase-match condition can be expressed as

$$n_{\text{eff}} \cdot \Lambda = n_f \cdot \Lambda \cdot sin\theta + N \cdot \lambda \tag{1}$$

where n_{eff} is the effective index of the mode propagating in the grating, n_f is the effective index of the fiber mode, λ is the operating wavelength, and N is the diffraction order. It should be noted that the incident angle can be either a positive angle or a negative angle. The incident angle is positive when the out-coupled wave has a component in the same direction as the input wave, as shown in shown in Fig. 2(a). The incident angle is negative when the out-coupled wave has a component in the opposite direction to the input wave, as shown in Fig. 2(b).

2.2. Uniform Gratings

The optimizations of our SWGCs with uniform grating periods were done using a finite-difference time-domain (FDTD) Maxwell equation solver combined with the particle swarm optimization algorithm [13] built in *FDTD Solutions*. Three parameters, the grating period, the width of the major grating, and the width of the subwavelength grating, as illustrated in Fig. 1(a), were optimized using 2-D simulations to achieve the lowest insertion loss. The polarization of the incident wave (PI), the operating wavelength (WI), the incident angle (Angle), the grating period (Period), the width of the major grating (Grating$_w$), and the width of the subwavelength grating (Sub$_w$) of the optimized SWGCs with uniform gratings are listed in Table 1.

2.3. Apodization

The out-coupled beam from a uniform SWGC has an exponentially decaying power $P = P_0 \cdot exp(-2\alpha z)$, where α is the leakage factor [14]. For an SWGC, the leakage factor can be tuned by changing the widths of the major gratings and/or the widths of the subwavelength gratings. Fig. 3 shows the leakage factor as a function of the widths of the subwavelength gratings and the major gratings for both the TE$_{00}$ and TM$_{00}$ modes. First, we fixed the width of the major gratings at the optimized value we obtained from the previous section and sweep the width of the subwavelength gratings, and then we fixed the width of the width of the subwavelength gratings to sweep the width of the major gratings. Comparing the curves in Fig. 3(a), we note that changing the widths of the subwavelength gratings gives us a larger tuning range for the leakage factor for the subwavelength TE grating coupler and comparing curves in Fig. 3(b), we note that the same applies this conclusion applies to the TM SWGCs. Therefore,

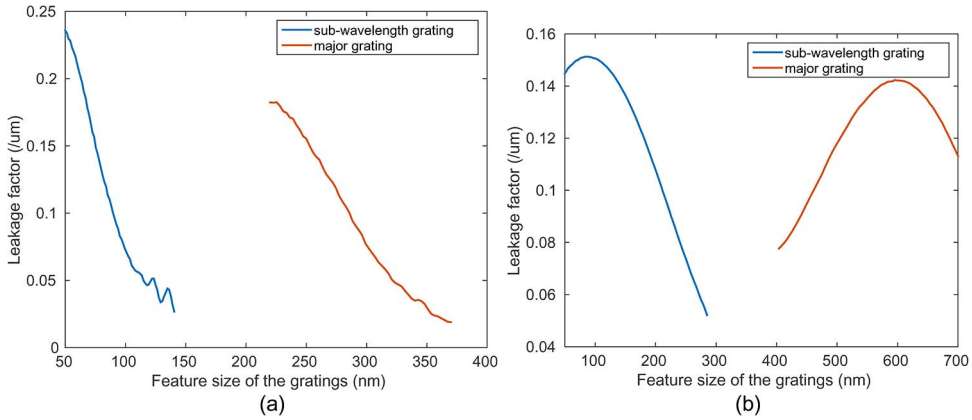

Fig. 3. (a) Leakage factor as a function of the width of the subwavelength grating and the width of the major grating for the subwavelength TE grating coupler. (b) Leakage factor as a function of the width of the subwavelength grating and the width of the major grating for the subwavelength TM grating coupler.

TABLE 2

Design parameters of the apodized regions for the SWGC TE and TM grating couplers

TE SWGC				TM SWGC			
P1 (nm)	480	Sub1 (nm)	120	P1 (nm)	895	Sub1 (nm)	220
P2 (nm)	516	Sub2 (nm)	120	P2 (nm)	895	Sub2 (nm)	189
P3 (nm)	500	Sub3 (nm)	120	P3 (nm)	917	Sub3 (nm)	173
P4 (nm)	521	Sub4 (nm)	120	P4 (nm)	914	Sub4 (nm)	200
P5 (nm)	500	Sub5 (nm)	120				
P6 (nm)	560	Sub6 (nm)	108				
P7 (nm)	500	Sub7 (nm)	100				
P8 (nm)	560	Sub8 (nm)	71				

we used the widths of the subwavelength gratings as the tuning factor to modify the leakage factor in our design.

To achieve a Gaussian output beam, 2α is given by [14]:

$$2\alpha(z) = \frac{G^2(z)}{1 - \int_0^z G^2(t)dt} \tag{2}$$

where $G(z)$ is a normalized Gaussian profile determined by the fiber mode and z is the propagation direction as shown in Fig. 2. With the relations shown in Fig. 3 and equation (2), we can get the required widths of the subwavelength gratings as a function of z. It should be noted that equation (3) is exact only for long gratings with small α, which is not the case for our structure. So we used the calculated widths of the subwavelength gratings as the starting point for further optimization. In order to achieve the phase-match condition between the adjacent grating periods, the periods of the subwavelength gratings also need to be modified. We applied particle swarm optimization on the width of the subwavelength grating and the grating period for each grating section to achieve the maximum output power. Each grating period has been treated as a separate grating section for optimization starting from the interface of the waveguide and the grating. The optimized grating period (P) and the width of the subwavelength grating (Sub) for each apodized grating section are shown in Table 2. Eight grating periods are required to be apodized for the TE SWGC and four grating periods are required to be apodized for the TM SWGC, which is due to the fact that the grating period of the TM SWGC is larger than that of the TE SWGC.

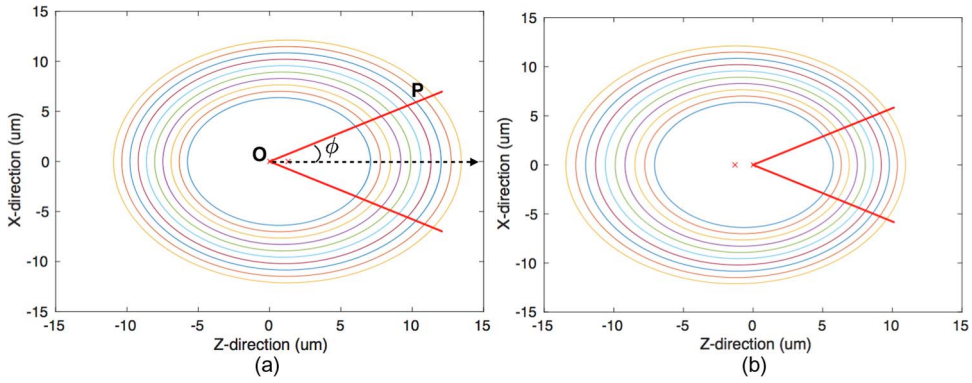

Fig. 4. Schematic of the focusing grating lines for SWGCs with (a) positive incident angles and (b) negative incident angles.

2.4. Focusing Grating Lines

So far, we have addressed the subwavelength grating as a two-dimension structure and equation (1) has assumed that the grating is linearly extended in the lateral (X) direction, where long adiabatic tapers are required. However, the long adiabatic tapers are not space efficient, consuming valuable on-chip real estate. Focusing grating lines are used as an alternative to achieve efficient mode size conversion [15]. The phase-match condition for a focusing SWGC can be expressed as

$$n_{\text{eff}} \cdot r = n_f \cdot r \cdot \sin\theta \cdot \cos\phi + N \cdot \lambda \tag{3}$$

where r denote the radius from the end of the silicon-wire waveguide (O as shown in Fig. 4) to an arbitrary point (P shown in Fig. 4) in the X-Z plan, ϕ denotes the angle between this radius and the z-axis. From (3), we can get the expression for r as:

$$r = \frac{N \cdot \lambda}{n_{\text{eff}} - n_f \cdot \sin\theta \cdot \cos\phi}. \tag{4}$$

Equation (4) defines a family of confocal ellipses with one of the focal points at the end of the waveguide. Schematics of the focusing grating lines for SWGCs are shown in Fig. 4. It should be noted that the grating pattern of the SWGCs with positive and negative incident angles are different. For SWGCs with positive incident angles, as shown in Fig. 4(a), the waveguide end overlaps with the left focal point of the confocal ellipses. For SWGCs with negative incident angles, as shown in Fig. 4(b), the waveguide end overlaps with the right focal point of the confocal ellipses.

A parameterized device cell has been created in *Mentor Graphics's Pyxis* [16] to generate the layout files for various SWGCs. The mask layouts were first exported from *Mentor Graphics*'s *Pyxis* and then imported into *FDTD Solutions* for 3-D simulation. Three-dimensional FDTD simulations were done for the focusing SWGCs for both the TE_{00} and the TM_{00} modes. These simulations have been done for both apodized and un-apodized SWGCs for comparison purposes. Fig. 5(a) shows the simulated transmission and reflection spectra of the apodized and un-apodized SWGCs for the TE_{00} mode. The apodized subwavelength TE grating coupler has an insertion loss of 2.1 dB, 0.6 dB lower than the un-apodized design, and a 1-dB bandwidth of 42 nm. The reflections from the apodized and un-apodized SWGCs are both below -20 dB. The apodized subwavelength TM grating coupler had an insertion loss of 2.2 dB, 0.7 dB lower than the un-apodized design, and a 1-dB bandwidth of 45 nm.

The principal loss in our SWGCs was the penetration loss to the substrate, which can be reduced by optimizing the thickness of the buried oxide or by adding a bottom mirror. The optimization of our design parameters were based on the silicon wafer used, which had a 220 nm

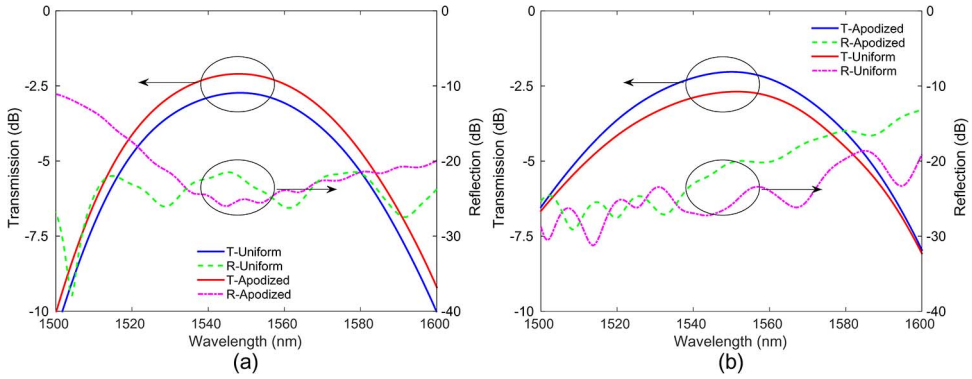

Fig. 5. (a) Simulated transmission spectra of the apodized and the un-apodized subwavelength TE grating couplers. (b) Simulated transmission spectra of the apodized and the un-apodized subwavelength TM grating couplers.

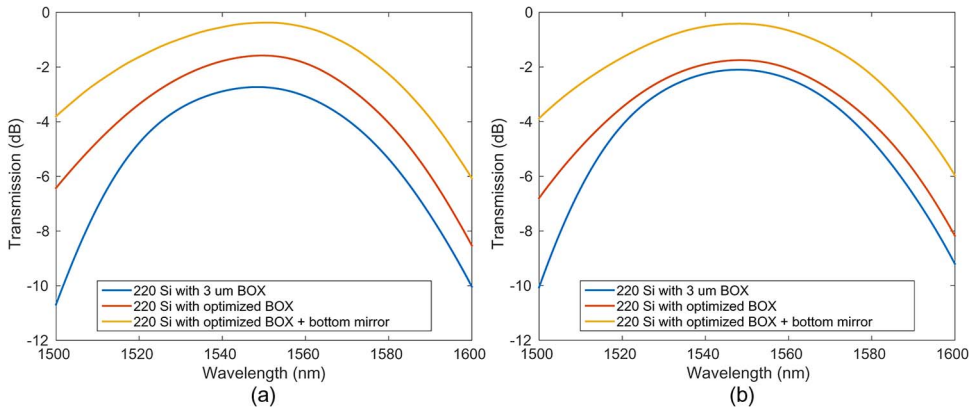

Fig. 6. (a) Simulated transmission spectra of the apodized subwavelength TE grating couplers. (b) Simulated transmission spectra of the apodized subwavelength TM grating coupler.

silicon layer and a 3 μm buried oxide layer. Both the silicon thickness and the buried oxide thickness were not optimized to achieve low insertion loss for our SWGCs. If we include the thickness of the buried oxide layer in our optimization process, then the insertion losses of the subwavelength TE and TM grating couplers can be improved to be 1.5 dB and 1.7 dB, respectively (shown in Fig. 6). Furthermore, if we include a bottom mirror (i.e., either a metal mirror or a Bragg reflector) in our SWGCs, then the insertion losses of our subwavelength TE and TM grating couplers can be as low as 0.34 dB and 0.41 dB, respectively (show in Fig. 6). The back reflections can be further reduced using the technique demonstrated in [17]. Given the fact that the back reflections of our SWGCs were low enough for our application, we did not use the technique in [17] to further reduce the back reflections. It should be noted that for the subwavelength TM grating coupler, apodization narrows the bandwidth of the grating period. According to [18], the bandwidth of the grating coupler is proportional to the period of the grating coupler. The grating period in the apodized region of the subwavelength TM grating coupler decreases from 960 nm to 872 nm, which causes the decrease in bandwidth. Compared to the TM grating coupler, the apodized periods of the subwavelength TE grating coupler only decreased from 556 nm to 505 nm. In addition, the back reflection from the apodized subwavelength TM grating coupler is larger than that of the un-apodized design, which is caused by the increased index contrast in the apodized region.

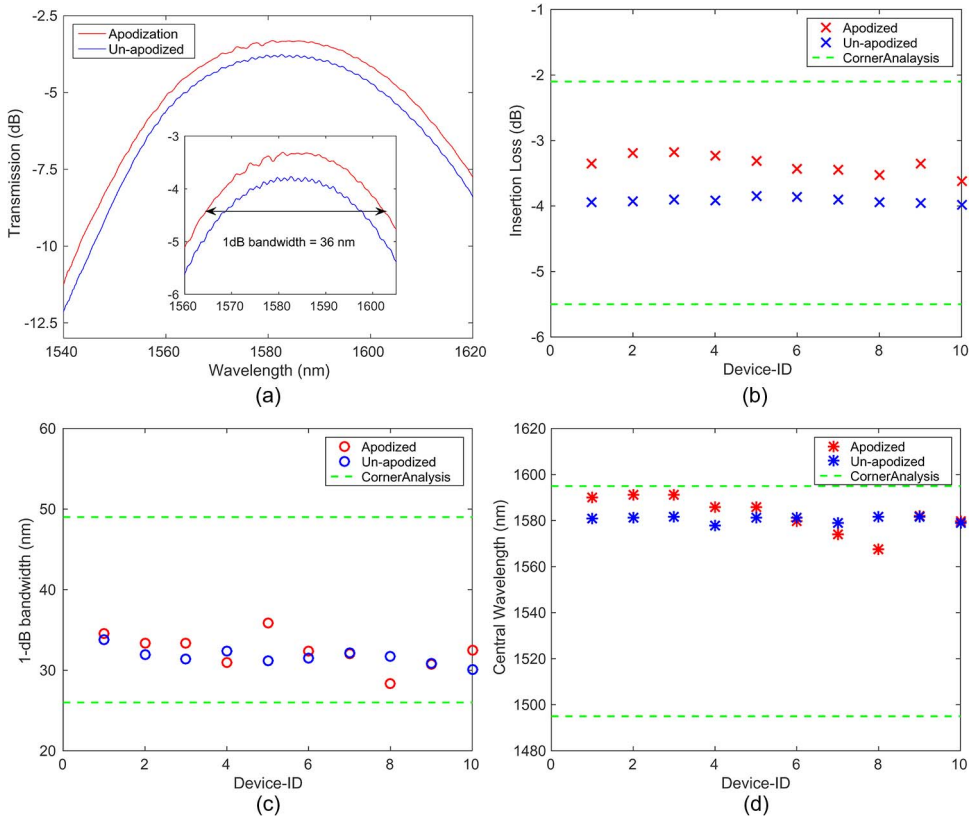

Fig. 7. (a) Measured spectra of an apodized and an un-apodized SWGC for the TE_{00} mode. (b) Insertion losses of apodized and un-apodized SWGCs for the TE_{00} mode. (c) 1-dB bandwidths of apodized and un-apodized SWGCs for the TE_{00} mode. (d) Central wavelengths of the apodized and un-apodized SWGC for the TE_{00} mode.

3. Fabrication and Measurement

The fabrication of the test structures for our SWGCs, consisting of an input SWGC and an output SWGC, with 127 μm pitch, connected by a silicon-wire waveguide were fabricated using electron beam lithography at the University of Washington [19]. Oxide cladding was used to cover the chip for protection. The fabricated devices were measured using our fiber-array-based automated measurement setup [20], the fiber array was polished at 23.2 degrees to accommodate the required incident angles for both the TE and TM designs.

3.1. Transverse Electric SWGC

Fig. 7 shows the calibrated measurement results for the subwavelength TE grating couplers. A large area detector was used to calibrate the loss from the measurement system, including the loss in the fiber array, the connectors, and the additional fibers used for extension. Fig. 7(a) shows the calibrated transmission spectra of apodized and un-apodized subwavelength TE grating couplers. The apodized design has an insertion loss of 3.2 dB, 0.6 dB better than the un-apodized one, with a 1-dB bandwidth of 36 nm, which is similar to that of the un-apodized design. The ripple at the central wavelength of the apodized subwavelength TE grating coupler is about 0.07 dB, which corresponds to a back reflection of -24 dB. The highly suppressed back reflection from our fully etched SWGC is comparable to state-of-art shallow etched grating couplers [2].

The same designs were fabricated multiple times on the same chip to test the performance stability. Fig. 7(b)–(d) shows the insertion losses, 1-dB bandwidths, and the central wavelengths of apodized and un-apodized subwavelength TE grating couplers having the same designs and

TABLE 3

Parameters used for corner analysis for SWGCs

Parameters	Angle	Grating_w	Sub_w	Si	BOX	SiO_2
Range	$\pm$ 2°	$\pm$ 10 nm	$\pm$ 10 nm	$\pm$ 10 nm	$\pm$ 20 nm	$\pm$ 100 nm

measured at different locations on a particular chip. It should be noted from this comparison, that, the stabilities of the insertion loss, the bandwidth, and the central wavelength of the un-apodized SWGCs were better than their stabilities for the apodized ones. This is the case because the apodized grating will only work if all of the apodized grating periods are in phase. Even a few nanometers offset in the widths of the subwavelength gratings can degrade the performance of the SWGC. Never the less, and despite the reduced stability, the average insertion loss of the apodized SWGCs was about 0.6 dB better than the average insertion loss of un-apodized SWGCs with similar bandwidths and central wavelengths.

Corner analysis has been applied to predict the range of the key characteristics of the as-designed grating couplers. Six parameters, i.e., the incident angle (Angle), the width of the major grating ($Grating_w$), the width of the subwavelength grating (Sub_w), the thickness of the silicon layer (Si), the thickness of the buried oxide (BOX), and the thickness of the oxide cladding (SiO_2), have been used in the corner analysis as shown in Table 3. The first three parameters shown in Table 3 mainly affect the central wavelength and the bandwidth of the grating coupler, and the last three parameters shown in Table 3 mainly affect the insertion loss of the grating coupler, since they change the interference condition of the light diffracted by the grating. The gap between the fiber tip and the chip surface is another important parameter that will affect the insertion loss and bandwidth of the grating couplers. Given the fact that we were using angle polished fibers and leaving sufficient space to avoid scratching the chip surface, the gap between the fiber core and the chip surface was kept at about 15 μm. A 15-μm gap was also used in the corner analysis (Table 3). According to our simulation, the extra insertion loss caused by this gap was about 0.5 dB. The measured insertion loss can be further reduced by polishing the fiber array to a particular angle so that the fiber tip and the chip surface can be parallel during the measurement. The dashed green lines in Fig. 7(b)–(d) denote the simulated boundaries in the corner analysis.

3.2 Transverse Magnetic SWGC

Fig. 8 shows the calibrated measurement results for the subwavelength TM grating couplers. Fig. 8(a) shows the measured transmission spectra of apodized and un-apodized subwavelength TM grating couplers. The apodized TM grating coupler has an insertion loss of 3.3 dB, 0.6 dB better than the un-apodized one, with a 1-dB bandwidth of 37 nm. The ripple at the central wavelength is about 0.15 dB, which corresponds to a back reflection of -21 dB. Fig. 8(b)–(d) shows the insertion losses, 1-dB bandwidths, and the central wavelengths of the apodized and un-apodized subwavelength TM grating couplers having the same designs and measured at different locations on a particular chip. Both the apodized and un-apodzied subwavelength TM grating couplers have good stability and reproducibility. This is the case because the TM mode is less sensitive than the TE mode to the design parameter change. The average insertion losses of the apodized designs are about 0.6 dB better than the average insertion loss of the un-apodized designs. Same corner analysis have been done for the TM SWGC, and a 30-μm gap was assumed in the simulation. The enlarged gap was caused by the increased angle difference between the polished angle and the required incident angle by the subwavelength TM grating couplers.

As compared to the measured spectral response of the TE SWGCs, an asymmetry can be observed in the spectral response of the TM SWGCs, which is due to the fact that the surface of the fiber tip and the grating surface were not parallel during the measurement. The fiber ribbon used in our measurement has a polish angle of 23.2°, which means that we need to tilt the

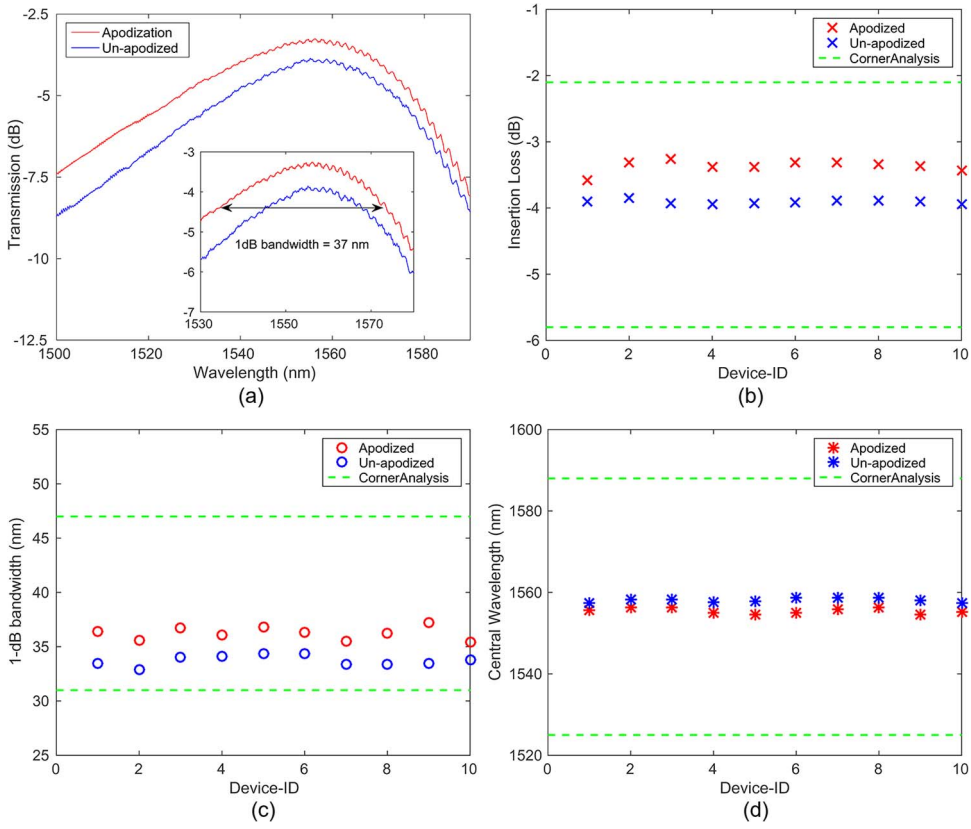

Fig. 8. (a) Measured spectra of an apodized and an un-apodized SWGC for the TM_{00} mode. (b) Insertion losses of apodized and un-apodized SWGCs for the TM_{00} mode. (c) 1-dB bandwidths of apodized and un-apodized SWGCs for the TM_{00} mode. (d) Central wavelengths of the apodized and un-apodized SWGCs for the TM_{00} mode.

fiber ribbon by 24° to get the required incident angle for the TM SWGCs. Therefore, an acute angle exists between the fiber tip and the surface of the grating. Incident waves at different wavelengths are diffracted at different angles by the grating. Longer wavelengths are not coupled into the fiber as efficiently as shorter wavelengths, which results in the asymmetry observed in the spectra.

4. Conclusion

We have experimentally demonstrated the apodized focusing SWGCs for both the TE_{00} and TM_{00} modes, which show a consistent improvement over the un-apodized designs. The differences between SWGCs with positive and negative incident angles have been illustrated, which is nontrivial to the design and fabrication of those SWGCs. Corner analysis have been applied to the SWGCs, which shows that our devices are robust considering the manufacturing variations assumed. As the resolution of the CMOS fabrication becomes smaller, those fully etched SWGCs can even become alternatives to the shallow-etched grating couplers; therefore, the fabrication cost and complexity can be reduced.

Acknowledgment

The devices were fabricated by Washington Nanofabrication Facility (WNF) at the University of Washington, part of the National Science Foundation National Nanotechnology Infrastructure Network (NNIN). The authors would like to thank Lumerical Solutions, Inc., and Mentor Graphics for the design software.

References

[1] W. S. Zaoui *et al.,* "Bridging the gap between optical fibers and silicon photonic integrated circuits," *Opt. Exp.*, vol. 22, no. 2, pp. 1277–1286, 2014.

[2] A. Mekis *et al.,* "A grating-coupler-enabled CMOS photonics platform," *IEEE J. Sel. Topics Quantum Electron.*, vol. 17, no. 3, pp. 597–608, May/Jun. 2011.

[3] D. Vermeulen *et al.,* "High-efficiency fiber-to-chip grating couplers realized using an advanced CMOS-compatible silicon-on-insulator platform," *Opt. Exp.*, vol. 18, no. 17, pp. 18 278–18 283, Aug. 2010.

[4] R. Halir *et al.,* "Continuously apodized fiber-to-chip surface grating coupler with refractive index engineered subwavelength structure," *Opt. Lett.*, vol. 35, no. 19, pp. 3243–3245, Oct. 2010.

[5] X. Xu *et al.,* "Colorless grating couplers realized by interleaving dispersion engineered subwavelength structures," *Opt. Lett.*, vol. 38, no. 18, pp. 3588–3591, Sep. 2013.

[6] Y. Ding, H. Ou, and C. Peucheret, "Ultra high-efficiency apodized grating coupler using fully etched photonic crystals," *Opt. Lett.*, vol. 38, no. 15, pp. 2732–2734, Aug. 2013.

[7] Y. Ding, C. Peucheret, H. Ou, and K. Yvind, "Fully etched apodized grating coupler on the SOI platform with −0.58 dB coupling efficiency," *Opt. Lett.*, vol. 39, no. 18, pp. 5348–5350, Sep. 2014.

[8] Z. Cheng *et al.,* "Focusing subwavelength grating coupler for mid-infrared suspended membrane waveguide," *Opt. Lett.*, vol. 37, no. 7, pp. 1217–1219, Apr. 2012.

[9] Z. Cheng, X. Chen, C. Y. Wong, K. Xu, and H. K. Tsang, "Apodized focusing subwavelength grating couplers for suspended membrane waveguides," *Appl. Phys. Lett.*, vol. 101, no. 10, Sep. 2012, Art. ID. 101104.

[10] Q. Zhong *et al.,* "Focusing-curved subwavelength grating couplers for ultra-broadband silicon photonics optical interfaces," *Opt. Exp.*, vol. 22, no. 15, pp. 18224–18231, Jul. 2014.

[11] Y. Wang *et al.,* "Focusing sub-wavelength grating couplers with low back reflections for rapid prototyping of silicon photonic circuits," *Opt. Exp.*, vol. 22, no. 17, pp. 20 652–20 662, Aug. 2014.

[12] R. Orobtchouk *et al.,* "High-efficiency light coupling in a submicrometric silicon-on-insulator waveguide," *Appl. Opt.*, vol. 39, no. 31, pp. 5773–5777, Nov. 2000.

[13] J. Robinson and Y. Rahmat-Samii, "Particle swarm optimization in electromagnetics," *IEEE Trans. Antennas Propag.*, vol. 52, no. 2, pp. 397–407, Feb. 2004.

[14] D. Taillaert, P. Bienstman, and R. Baets, "Compact efficient broadband grating coupler for silicon-on-insulator waveguides," *Opt. Lett.*, vol. 29, no. 23, pp. 2749–2751, Dec. 2004.

[15] F. Van Laere *et al.,* "Compact focusing grating couplers for silicon-on-insulator integrated circuits," *IEEE Photon. Technol. Lett.*, vol. 19, no. 23, pp. 1919–1921, Dec. 2007.

[16] L. Chrostowski *et al.,* "Design methodologies for silicon photonic integrated circuits," in *Proc. SPIE OPTO*, Mar. 2014, Art. ID. 89890G.

[17] D. Vermeulen *et al.,* "Reflectionless grating couplers for silicon-on-insulator photonic integrated circuits," *Opt. Exp.*, vol. 20, no. 20, pp. 22 278–22 283, Sep. 2012.

[18] X. Chen, K. Xu, Z. Cheng, C. K. Fung, and H. K. Tsang, "Wideband subwavelength gratings for coupling between silicon-on-insulator waveguides and optical fibers," *Opt. Lett.*, vol. 37, no. 17, pp. 3483–3485, Sep. 2012.

[19] R. J. Bojko *et al.,* "Electron beam lithography writing strategies for low loss, high confinement silicon optical waveguides," *J. Vacuum Sci. Technol. B*, vol. 29, no. 6, Nov./Dec. 2011, Art. ID. 06F309.

[20] Y. Wang *et al.,* "Fully etched grating coupler with low back reflection," in *Proc. SPIE Photon. North*, Oct. 2013, Art. ID. 89150U.